JOURNAL OF GEOPHYSICAL RESEARCH, VOL. 115, A02213, doi:10.1029/2009JA014580, 2010

Particle-in-cell simulations of whistler waves excited by an electron κ distribution in space plasma

Quanming Lu,[1,2] Lihui Zhou,[1,2] and Shui Wang[1]

Received 19 June 2009; revised 6 September 2009; accepted 29 September 2009; published 26 February 2010.

[1] Satellite observations clearly reveal that superthermal electrons in space plasma generally possess a pronounced non-Maxwellian distribution that can be well modeled by a κ distribution. In this paper, one-dimensional (1-D) particle-in-cell simulations are performed to investigate the evolution of whistler waves driven by superthermal electrons with a typical κ distribution in the presence of a cold plasma population. The results obtained from the linear theory are first confirmed: with the increase of the spectral index κ for the κ distribution, the linear growth rate of the excited waves increases and instability threshold for the temperature anisotropy ($A = T_\perp/T_\parallel - 1$) decreases. Then we further find that with the increase of κ, the fluctuating magnetic field energy density at the saturation stage also increases. Therefore, from both the linear growth rate and the fluctuating magnetic field energy density at the saturation stage, we can find that a bi-Maxwellian distribution ($\kappa \rightarrow \infty$) overestimates the importance of whistler waves, since the observed value of κ lies in the range $2 \leq \kappa \leq 6$. We also find that the κ values of the electron distributions become smaller with the excitation of the whistler waves.

Citation: Lu, Q., L. Zhou, and S. Wang (2010), Particle-in-cell simulations of whistler waves excited by an electron κ distribution in space plasma, *J. Geophys. Res.*, *115*, A02213, doi:10.1029/2009JA014580.

1. Introduction

[2] Whistler mode waves at frequencies below the electron cyclotron frequency are an important constituent of magnetospheric plasmas. There is increasing evidence that whistler waves may contribute to energization of relativistic electrons in the outer radiation belt during geomagnetic storms through resonant wave-particle interactions, and these energetic electrons yield failures and malfunctions of geostationary spacecraft [e.g., *Horne and Thorne*, 1998; *Meredith et al.*, 2002; *Horne et al.*, 2005; *Summers et al.*, 1998, 2007; *O'Brien et al.*, 2004; *Shprits et al.*, 2006; *Thorne et al.*, 2005, 2007; *Li et al.*, 2007; *Tao et al.*, 2008]. These waves are generally considered to be excited by anisotropic electrons and to then give rise to enhanced fluctuating magnetic field, which in turn leads to wave-particle scattering and reduces the anisotropy [*Katoh and Omura*, 2004, 2007; *Omura et al.*, 2008].

[3] Whistler waves excited by an electron temperature anisotropy, where electrons are assumed to satisfy a bi-Maxwellian distribution with an anisotropy $A = T_\perp/T_\parallel - 1 > 0$ (where $T_\perp$ and $T_\parallel$ are the electron temperatures perpendicular and parallel to the background magnetic field, respectively, and $\perp$ and $\parallel$ denote the directions perpendicular and parallel to the background magnetic field $\mathbf{B}_0$), have been investigated in numerous papers with both the linear theory and computer simulations [*Gary and Wang*, 1996; *Gary and Cairns*, 1999; *Nishimura et al.*, 2002; *Gary and Karimabadi*, 2006]. The linear theory has shown that there exists a minimum temperature anisotropy termed the instability threshold [*Gary and Wang*, 1996; *Gary and Cairns*, 1999; *Nishimura et al.*, 2002]. Whistler mode waves are unstable when the electron temperature anisotropy is larger than the threshold, and this threshold corresponds to the onset of strong wave-particle interactions. In a homogeneous plasma, the fastest growing whistler mode excited by the temperature anisotropy propagates along the background magnetic field. According to the linear theory, the instability threshold for this growing mode can be described as [*Gary and Wang*, 1996]

$$A = \frac{T_\perp}{T_\parallel} - 1 = \frac{S}{\beta_\parallel^\alpha}, \tag{1}$$

where $\beta_\parallel = 8\pi\, n_e\, T_\parallel/B_0^2$ and n_e is the electron density. S and α are two fitting parameters, and they can be determined by the following procedure: A threshold value for the maximum growth rate $\gamma_m/|\Omega_e|$ (where $\Omega_e = eB_0/m_e c$ is the electron cyclotron frequency) is first chosen, and then according to the linear theory, the temperature anisotropies for the instability can be calculated on a specific range of $\beta_\parallel$ values; at last, a least squares fit is used to determine the values of S and α. S varies as a function of the chosen threshold for the maximum growth rate, while α is almost independent of the

[1]CAS Key Laboratory of Basic Plasma Physics, School of Earth and Space Sciences, University of Science and Technology of China, Hefei, China.
[2]State Key Laboratory of Space Weather, Chinese Academy of Sciences, Beijing, China.

0148-0227/10/2009JA014580$09.00

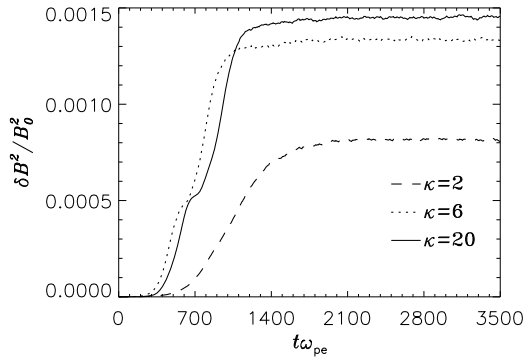

Figure 1. The evolution of fluctuating magnetic field energy densities $\delta B^2/B_0^2$ for $\kappa = 2$ (dashed line), $\kappa = 6$ (dotted line), and $\kappa = 20$ (solid line).

chosen threshold growth rate. Particle-in-cell (PIC) simulations have also been performed to investigate whistler waves excited by the electron temperature anisotropy [*Devine et al.*, 1995; *Gary et al.*, 2000; *Lu et al.*, 2004], and these simulations verified that such a threshold represents an approximate constraint on the electron anisotropy. At the same time, such a threshold also imposes an upper bound on the electron anisotropy in a space plasma environment, owing to pitch angle scattering by the excited whistler waves [*Gary et al.*, 2005]. With the measurements from the Plasma Electron and Current Experiment (PEACE) instruments on the Cluster 1 spacecraft, *Gary et al.* [2005] found that electron anisotropies in the dayside terrestrial magnetosheath are constrained statistically by the upper bound given by equation (1) and implicated that such a constraint should be applied in other sufficiently collisionless and homogeneous space and astrophysical bi-Maxwellian plasma environments. PIC simulations further found that during the nonlinear evolution stage of whistler waves excited by the electron bi-Maxwellian distribution, the dominant mode (whose amplitude has the maximum value) drifts from high frequency to low values [*Devine et al.*, 1995; *Lu et al.*, 2004].

[4] However, in various space plasma environments, for example, the Earth's foreshock region and outer radiation belts, the plasma is ubiquitously observed to be characterized by a small population of electrons with a suprathermal tail distribution [*Vasyliunas*, 1968; *Gosling et al.*, 1981; *Lin et al.*, 1981, 1986; *Fitzenreiter et al.*, 1998, 1990; *Fu et al.*, 2006]. Such a distribution can be well modeled by the so-called generalized Lorentzian (κ) function [*Vasyliunas*, 1968; *Summers and Thorne*, 1991; *Yin et al.*, 1998; *Xiao*, 2006; *Xiao et al.*, 2008; *Yoon et al.*, 2006]. Recently, with the linear theory, *Xiao et al.* [2006] investigated the whistler instability driven by a population of suprathermal electrons with an anisotropy ($A = T_\perp/T_\parallel - 1 > 0$) in the presence of a cold, dense electron population and found that the anisotropy of the suprathermal electrons can be modeled by a κ distribution. *Xiao et al.* [2006] found that the instability threshold for the κ distribution generally decreases as the spectral index κ increases and tends to the lowest limiting value of the bi-Maxwellian distribution as $\kappa \to \infty$. In this paper, one-dimensional (1-D) PIC simulations are performed to study the nonlinear evolution of the whistler instability driven by a population of superthermal electrons with a κ distribution. Not only the linear growth rate but also the fluctuating magnetic field energy density at the saturation stage is discussed.

[5] The paper is organized as follows. Section 2 presents the simulation model and plasma conditions. Section 3 describes the simulation results, and section 4 summarizes the discussion and conclusions.

2. Simulation Model

[6] We perform 1-D electromagnetic PIC simulations to investigate the nonlinear evolution of the whistler instability driven by a population of suprathermal electrons with a κ distribution in the presence of a cold plasma population, where periodic boundary conditions are used in the simulations. Only electrons move in the simulations, and the ion dynamics are neglected. The 1-D simulations allow spatial variations only in the x direction with a uniform background magnetic field $\mathbf{B}_0 = B_0\,\hat{\mathbf{x}}$ (where $\hat{\mathbf{x}}$ is the unit vector along the x direction). It is reasonable to study the evolution of the whistler waves with 1-D PIC simulations, since whistler waves usually propagate along the direction of the background magnetic field.

[7] Initially, two electron populations are employed in the simulations. One is the cold, dense electron population with the density n_c and a velocity distribution that satisfies an isotropic Maxwellian function with the temperature T_c. The other is the tenuous population of suprathermal electrons with a κ distribution and the density n_s. The background neutralizing ions have the density $n_i = n_c + n_s$. Here, we choose $n_s/n_i = 0.05$. The κ distribution of the suprathermal electrons can be modeled as [*Summers and Thorne*, 1991; *Xiao et al.*, 2006]

$$f^\kappa(v_\parallel, v_\perp) = \frac{n_s\Gamma(\kappa+1)}{\pi^{3/2}\theta_\perp^2\theta_\parallel\kappa^{3/2}\Gamma(\kappa-1/2)}\left[1+\frac{v_\parallel^2}{\kappa\theta_\parallel^2}+\frac{v_\perp^2}{\kappa\theta_\perp^2}\right]^{-(\kappa+1)}, \tag{2}$$

and the corresponding parallel and perpendicular effective thermal speeds are

$$\theta_\parallel = [(2\kappa-3)/\kappa]^{1/2}\left(\frac{T_\parallel}{m_e}\right)^{1/2}, \tag{3}$$

$$\theta_\perp = [(2\kappa-3)/\kappa]^{1/2}\left(\frac{T_\perp}{m_e}\right)^{1/2}, \tag{4}$$

where Γ is the gamma function and m_e is the mass of the electrons. $T_\parallel$ and $T_\perp$ are the electron temperatures parallel and perpendicular to the background magnetic field $\mathbf{B}_0$, respectively. The temperature anisotropy of the suprathermal electrons is

$$A = \frac{T_\perp}{T_\parallel} - 1 = \frac{\theta_\perp^2}{\theta_\parallel^2} - 1. \tag{5}$$

The κ distribution with $2 \le \kappa \le 6$ generally provides a good representation of the suprathermal electrons in various space

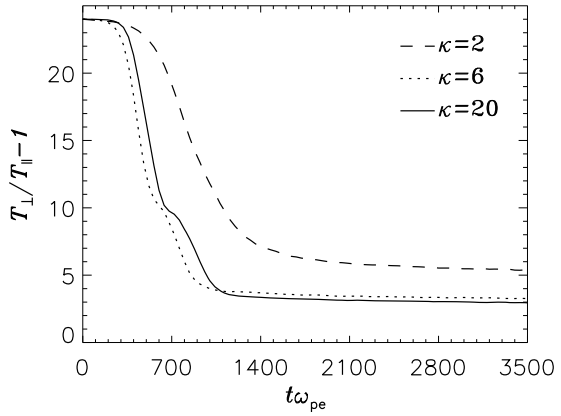

Figure 2. The evolution of the temperature anisotropies of the superthermal electrons $A = T_\perp/T_\parallel - 1$ for $\kappa = 2$ (dashed line), $\kappa = 6$ (dotted line), and $\kappa = 20$ (solid line).

plasma environments [*Vasyliunas*, 1968; *Summers and Thorne*, 1991]. The κ distribution also contains the well-known standard Maxwellian distribution f^M as $\kappa \to \infty$ in equations (2)–(4), where

$$f^M(v_\parallel, v_\perp) = \frac{n_s}{\pi^{3/2} a_\perp^2 a_\parallel} \exp\left[-\frac{v_\parallel^2}{a_\parallel^2} - \frac{v_\perp^2}{a_\perp^2}\right]. \quad (6)$$

As $\kappa \to \infty$, $\theta_\parallel \to a_\parallel$, $\theta_\perp \to a_\perp$, and $f^\kappa \to f^M$. Values $a_\parallel$ and $a_\perp$ are the parallel and perpendicular thermal speeds:

$$a_\parallel = \left(\frac{2T_\parallel}{m_e}\right)^{1/2}, a_\perp = \left(\frac{2T_\perp}{m_e}\right)^{1/2}. \quad (7)$$

In the simulations, the densities are normalized to the ion density n_i, and the velocities are expressed in units of the thermal speed of the cool electron population with an isotropic Maxwellian distribution $v_{Tc} = (T_c/m_e)^{1/2}$. Space and time are expressed in units of the Debye length $\lambda_D = (T_c/4\pi n_i e^2)^{1/2}$ and the inverse of the plasma frequency $\omega_{pe} = (4\pi n_i e^2/m_e)^{1/2}$, respectively. The electric and magnetic fields are normalized to $m_e\omega_{pe}v_{Tc}/e$ and $m_e\omega_{pe}c/e$, respectively. The grid size Δx is chosen as λ_D, and the time step is $\omega_{pe}\Delta t = 0.004$. The number of grids used in the simulation is 2048, and there are 200 superparticles per cell for each electron population. One superparticle in the simulations represents a number of particles with similar properties in reality. The domain size is $L = 2048\lambda_D$ if no explicit statement is given. The light speed is assumed to be $c = 120v_{Tc}$. The expression $1/\eta_e = \Omega_e/\omega_{pe}$ is chosen to represent the strength of magnetic fields.

3. Simulation Results

[8] The linear theory has predicted that the κ distribution with an anisotropy $A = T_\perp/T_\parallel - 1 > 0$ can excite whistler waves propagating along the background magnetic field. At the same time, with the increase of κ the linear growth rate of the excited waves increases and instability threshold for the temperature anisotropy decreases [*Xiao et al.*, 2006]. In this paper, we first present an ensemble of simulations with the initial values $1/\eta_e = \Omega_e/\omega_{pe} = 0.3$ and $T_{\perp 0}/T_{\parallel 0} - 1 = 24$ (where $T_{\perp 0}$ and $T_{\parallel 0}$ are the initial electron temperatures perpendicular and parallel to the background magnetic field, respectively) for the superthermal electrons. In the simulations, a larger temperature anisotropy $T_{\perp 0}/T_{\parallel 0} - 1 = 24$ is used in order to investigate the evolution of the instabilities more clearly. Although it will increase the linear growth rate and saturation level of the fluctuating magnetic field energy density, the evolution trend of the excited waves will not change. Initially, the superthermal electrons are assumed to satisfy a κ distribution, and three different values of κ are used in the simulations. Figure 1 shows the evolution of fluctuating magnetic field energy densities for different values of κ. The whistler waves begin to be excited at about $t\omega_{pe} = 500$ and then undergo a linear growth stage. A saturation stage is approached at about $t\omega_{pe} = 2000$ for $\kappa = 2$ and $t\omega_{pe} = 1300$ for $\kappa = 6$ or $\kappa = 20$. In general, the fluctuating magnetic field energy densities at the saturation stage increase with the increase of κ, which are about $\delta B^2/B_0^2 = 0.00080$, 0.00132, and 0.00146 for $\kappa = 2$, 6, and 20, respectively. However, no further obvious enhancement of the fluctuating magnetic field energy density can be found after κ is raised to be larger than ~6. At the same time, with the excitation of the electromagnetic waves, the waves can scatter the superthermal electrons, which reduces their perpendicular temperature and increases their parallel temperature. Therefore, the temperature anisotropy decreases. Figure 2 illustrates the evolution of the temperature anisotropies of the superthermal electrons for different κ. At about

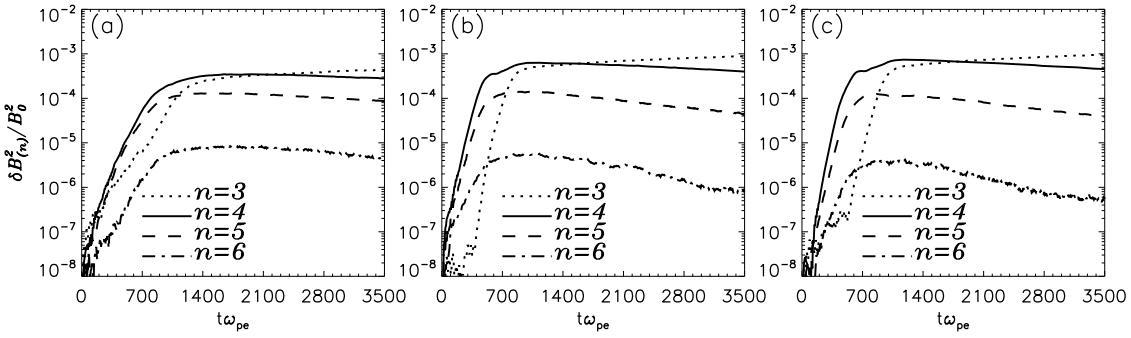

Figure 3. The evolution of the fluctuating magnetic energy densities corresponding to four main modes $\delta B^2_{(n)}/B_0^2$ with the four largest amplitudes for (a) $\kappa = 2$, (b) $\kappa = 6$, and (c) $\kappa = 20$. The mode number n corresponds to wave number $k = 2\pi n/L$. The wave numbers are about $kc/\omega_{pe} \approx 1.10$ (dotted line), 1.48 (solid line), 1.84 (dashed line), and 2.21 (dash-dotted line), respectively.

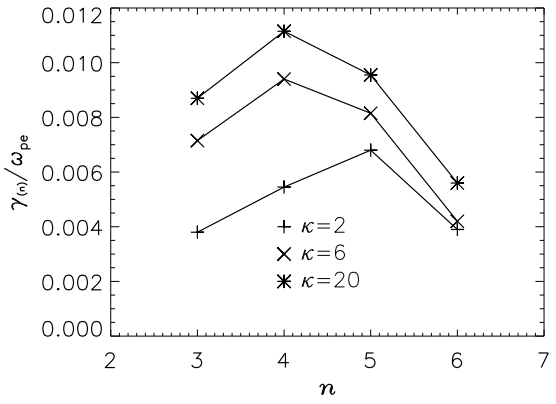

Figure 4. The linear growth rates $\gamma_{(n)}$ for κ = 2 (pluses), κ = 6 (crosses), and κ = 20 (asterisks) at mode numbers n = 3, 4, 5, and 6. The solid lines connect different points at different mode numbers.

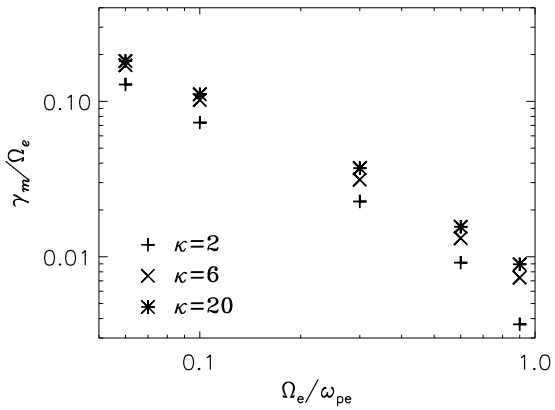

Figure 6. The maximum linear growth rates γ_m for five different runs with range $1/\eta_e = \Omega_e/\omega_{pe}$ = 0.06~0.9 and for κ = 2 (pluses), κ = 6 (crosses), and κ = 20 (asterisks). The initial temperature anisotropy $T_{\perp 0}/T_{\|0} - 1 = 24$ is used for the superthermal electrons.

$t\omega_{pe}$ = 500, with the excitation of the whistler waves, the anisotropies of the superthermal electrons decrease. At the saturation stage, the temperature anisotropies almost do not change, which are ~5.4, 3.3, and 3.0 for κ = 2, 6, and 10, respectively.

[9] The above analysis only illustrates the evolution of the total fluctuating magnetic field energy densities excited by the superthermal electrons with a κ distribution. However, actually the superthermal electrons excite whistler waves with a spectrum. In order to know the characteristics of different wave modes, in Figure 3 we describe the evolution of the fluctuating magnetic energy densities corresponding to four main modes with the four largest amplitudes. In Figure 3, three different κ are used (κ = 2, κ = 6, and κ = 20), and the mode number n corresponds to wave number $k = 2\pi\, n/L$. Therefore, the wave numbers are about 0.0092 λ_D^{-1}, 0.0123λ_D^{-1}, 0.0153λ_D^{-1}, and 0.0184λ_D^{-1} for mode numbers n = 3, 4, 5, and 6, respectively, which correspond to $kc/\omega_{pe} \approx$ 1.10, 1.48, 1.84, and 2.21. The linear growth rates for different κ at different mode numbers are plotted in Figure 4. For κ = 6 and κ = 20, the mode with n = 4 has the maximum growth rate, while the mode n = 5 has the maximum growth rate for κ = 2. At the same time, the maximum growth rate increases with the increase of κ. The basic reason for this is that the maximum wave growth is generally determined by the velocity space gradients [*Xue et al.*, 1996], which tend to be smaller as κ is lowered. In the saturation stage, at first the mode n = 4 has the largest amplitude; then the amplitude of the mode n = 3 increases gradually and becomes dominant at the end of the simulations. This can be demonstrated more clearly in Figure 5, which shows the magnetic field energy densities for mode number n = 1 ~ 10 at $t\omega_{pe}$ = 3500. At that time, the amplitude of the fluctuating magnetic field $\delta B_{(n)}^2/B_0^2$ for mode number n = 3 is ~0.00044, 0.00088, and 0.00097 for κ = 2, 6, and 10, respectively. The above results show that during the nonlinear evolution, the frequency of the dominant mode (with the largest amplitude) drifts to small values, and it is similar to the previous simulations where the superthermal electrons are assumed to have a bi-Maxwellian distribution [*Devine et al.*, 1995; *Lu et al.*, 2004]. The drift of the dominant mode to small values is attributed to the decrease of the frequency of the dominant mode with decreasing anisotropy $A = T_\perp/T_\| - 1$ [*Ossakow et al.*, 1972]; then as the simulation progresses (A decreases in time), the range of the available resonant modes decreases. Similar phenomena can also be found for ion cyclotron waves excited by ion temperature anisotropies [*Lu et al.*, 2006].

[10] Then we investigate the influences of the background magnetic field on the excited whistler waves for different κ.

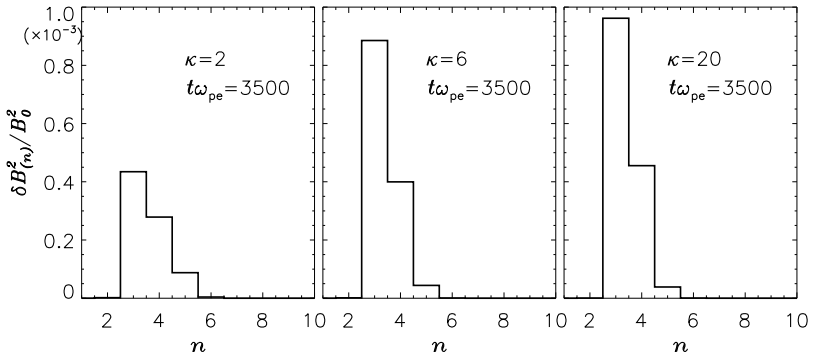

Figure 5. The magnetic field energy densities $\delta B_{(n)}^2/B_0^2$ at mode number n = 1~10 at $t\omega_{pe}$ = 3500 for (left) κ = 2, (middle) κ = 6, and (right) κ = 20.

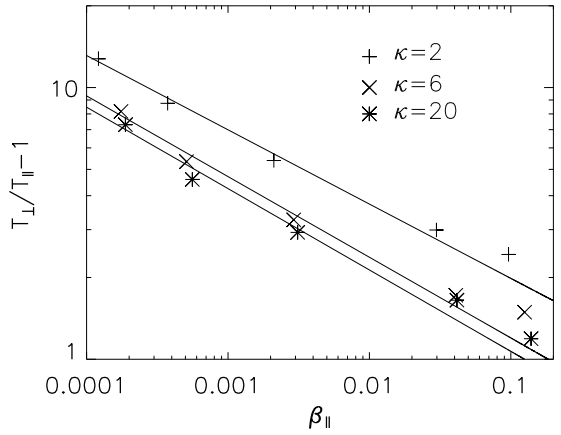

Figure 7. The temperature anisotropies $A = T_\perp/T_\parallel - 1$ at the saturation stage for five different runs versus $\beta_\parallel = 8\pi n_h T_\parallel/B_0^2 = (\omega_{pe}/\Omega_e)^2\,(2T_\parallel/m_e c^2)$ for $\kappa = 2$ (pluses), $\kappa = 6$ (crosses), and $\kappa = 20$ (asterisks). $T_\parallel$ is the parallel temperature at the saturation stage. The solid lines are least squares fits to the corresponding points. The initial temperature anisotropy $T_{\perp 0}/T_{\parallel 0} - 1 = 24$ is used for the superthermal electrons.

Figure 6 illustrates the maximum linear growth rates for five different runs with range $1/\eta_e = \Omega_e/\omega_{pe} = 0.06$~$0.9$ and for $\kappa = 2$, $\kappa = 6$, and $\kappa = 20$. In all runs; the initial temperature anisotropy $T_{\perp 0}/T_{\parallel 0} - 1 = 24$ is used for the superthermal electrons. Obviously, in all these cases the maximum linear growth rate decreases with the decrease of κ, and it seems that the influence of κ on the maximum linear growth rate becomes large with the increase of Ω_e/ω_{pe}. We can again verify that there is no further obvious increase of the maximum linear growth rates when κ is larger than 6 in the range $1/\eta_e = \Omega_e/\omega_{pe} = 0.06$~$0.9$.

[11] Figure 7 shows the temperature anisotropies at the saturation stage for five different runs versus $\beta_\parallel = 8\pi\, n_s T_\parallel/B_0^2 = (\omega_{pe}/\Omega_e)^2\,(2T_\parallel/m_e\, c^2)$ for $\kappa = 2$, $\kappa = 6$, and $\kappa = 20$. $T_\parallel$ is the parallel temperature at the saturation stage. As demonstrated by *Gary and Wang* [1996], the temperature anisotropy at the saturation stage can be used as an approximation of the threshold for the instability excited by the superthermal electrons with a κ distribution. Obviously, with the increase of κ, the instability threshold decreases, and the whistler waves are easier to be excited [*Xiao et al.*, 2006]. At the same time, with the increase of the background magnetic field, the instability threshold also increases, and the waves are difficult to be excited.

Table 1. The κ Values of the Electron Distributions at the Saturation Stages

$1/\eta_e = \Omega_e/\omega_{pe}$	κ
0.06	1.7
0.1	1.7
0.3	2.5
0.6	3.9
0.9	5.5

[12] The threshold for the instability excited by the superthermal electrons with a κ distribution has the form [*Xiao et al.*, 2006]

$$\frac{T_\perp}{T_\parallel} - 1 = \frac{S}{\beta_\parallel^\alpha}. \tag{8}$$

Here S and α are fitting parameters, and $T_\parallel$ is the parallel temperature at the saturation stage. By doing a least squares fit, we can calculate that at $\kappa = 2$, $S = 1.06$ and $\alpha = 0.27$; at $\kappa = 6$, $S = 0.6$ and $\alpha = 0.29$; and at $\kappa = 20$, $S = 0.53$ and $\alpha = 0.30$. The results are consistent with the linear theory [*Xiao et al.*, 2006], which predicts $0.25 \le \alpha \le 0.52$.

[13] We also investigate the evolution of electron velocity distributions. Figures 8a and 8b describe the electron velocity distributions at $t\omega_{pe} = 0$ and $t\omega_{pe} = 3500$, respectively, for $1/\eta_e = \Omega_e/\omega_{pe} = 0.3$ and $\kappa = 20$. The initial temperature anisotropy $T_{\perp 0}/T_{\parallel 0} - 1 = 24$ is used for the superthermal electrons. At the saturation stage ($t\omega_{pe} = 3500$), the perpendicular temperature is smaller than its initial value, and the parallel temperature is larger than its initial value. By doing a least squares fit of the electron distribution at the saturation stage to a κ distribution, the κ value is ~2.5. Table 1 shows the κ values of the electron distributions at the saturation stage for different $1/\eta_e = \Omega_e/\omega_{pe}$. In all runs, the initial temperature anisotropy $T_{\perp 0}/T_{\parallel 0} - 1 = 24$ is used for the superthermal electrons, and κ is 20. Obviously, the κ values

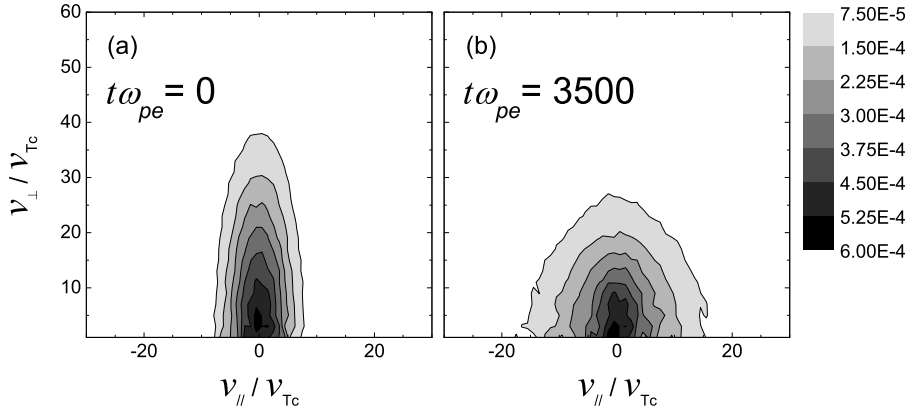

Figure 8. The electron velocity distributions for $1/\eta_e = \Omega_e/\omega_{pe} = 0.3$ and $\kappa = 20$ at (a) $t\omega_{pe} = 0$ and (b) $t\omega_{pe} = 3500$. The initial temperature anisotropy $T_{\perp 0}/T_{\parallel 0} - 1 = 24$ is used for the superthermal electrons.

at the saturation stage become large with the increase of $1/\eta_e = \Omega_e/\omega_{pe}$. Similar results are obtained if the initial κ values are chosen as 2 or 6.

4. Discussion and Conclusions

[14] In this paper, we used a 1-D PIC simulation to study the evolution of whistler waves driven by superthermal electrons with a typical κ distribution in the presence of a cold plasma population. The variations of the instability with the spectral index κ are investigated. At first, we confirmed the results of the linear theory, which demonstrates that with the increase of κ the linear growth rate of the waves increases and the instability threshold for the temperature anisotropy decreases. Then, we further find that the fluctuating magnetic field energy at the saturation stage also increases as κ increases. Hence the results by a bi-Maxwellian distribution ($\kappa \rightarrow \infty$) generally overestimate the importance of whistler waves (the saturation amplitude, as well as the linear growth rate), since observed values of κ lie in the range $2 \leq \kappa \leq 6$ for a typical κ distribution in space plasma. It is also found that during the nonlinear evolution of excited waves the dominant mode drifts from a high frequency to low frequencies as in a bi-Maxwellian distribution plasma [*Devine et al.*, 1995; *Lu et al.*, 2004]. At the same time, with the increase of the background magnetic field, the instability threshold for the electron temperature anisotropy also increases, and the whistler waves are difficult to be excited by a κ distribution. The κ values of the electron distributions are found to become smaller with the excitation of the whistler waves.

[15] **Acknowledgments.** This research was supported by Chinese Academy of Sciences grant KJCX2-YW-N28; National Science Foundation of China (NSFC) grants 40874075, 40674093, and 40725013; and the Specialized Research Fund for State Key Laboratories.

[16] Zuyin Pu thanks the reviewers for their assistance in evaluating this paper.

References

Devine, P. E., S. C. Chapman, and J. W. Eastwood (1995), One- and two-dimensional simulations of whistler mode waves in an anisotropic plasma, *J. Geophys. Res.*, *100*, 17,189, doi:10.1029/95JA00842.

Fitzenreiter, R. J., J. D. Scudder, and A. J. Klimas (1990), Three-dimensional analytical model for the spatial variation of the foreshock electron distribution function: Systematics and comparisons with ISEE observations, *J. Geophys. Res.*, *95*, 4155, doi:10.1029/JA095iA04p04155.

Fitzenreiter, R. J., K. W. Ogilvie, D. J. Chornay, and J. Keller (1998), Observations of electron velocity distribution functions in the solar wind by the WIND spacecraft: High angular resolution Strahl measurements, *Geophys. Res. Lett.*, *25*, 249, doi:10.1029/97GL03703.

Fu, X. R., Q. M. Lu, and S. Wang (2006), The process of electron acceleration during collisionless magnetic reconnection, *Phys. Plasmas*, *13*, 012309, doi:10.1063/1.2164808.

Gary, S. P., and I. H. Cairns (1999), Electron temperature anisotropy instabilities: Whistler, electrostatic and z mode, *J. Geophys. Res.*, *104*, 19,835, doi:10.1029/1999JA900296.

Gary, S. P., and H. Karimabadi (2006), Linear theory of electron temperature anisotropy instabilities: Whistler, mirror, and Weibel, *J. Geophys. Res.*, *111*, A11224, doi:10.1029/2006JA011764.

Gary, S. P., and J. Wang (1996), Whistler instability: Electron anisotropy upper bound, *J. Geophys. Res.*, *101*, 10,749, doi:10.1029/96JA00323.

Gary, S. P., D. Winske, and M. Hesse (2000), Electron temperature anisotropy instabilities: Computer simulations, *J. Geophys. Res.*, *105*, 10,751, doi:10.1029/1999JA000322.

Gary, S. P., B. Lavraud, M. F. Thomsen, B. Lefebvre, and S. J. Schwartz (2005), Electron anisotropy constraint in the magnetosheath: Cluster observations, *Geophys. Res. Lett.*, *32*, L13109, doi:10.1029/2005GL023234.

Gosling, J. T., J. R. Asbridge, S. J. Bame, W. C. Feldman, R. D. Zwickl, G. Paschmann, N. Sckopke, and R. J. Hynds (1981), Interplanetary ions during an energetic storm particle event: The distribution function from solar wind thermal energies to 1.6 MeV, *J. Geophys. Res.*, *86*, 547, doi:10.1029/JA086iA02p00547.

Horne, R. B., and R. M. Thorne (1998), Potential waves for relativistic electron scattering and stochastic acceleration during magnetic storms, *Geophys. Res. Lett.*, *25*, 3011, doi:10.1029/98GL01002.

Horne, R. B., R. M. Thorne, S. A. Glauert, J. M. Albert, N. P. Meredith, and R. R. Anderson (2005), Timescale for radiation belt electron acceleration by whistler mode chorus waves, *J. Geophys. Res.*, *110*, A03225, doi:10.1029/2004JA010811.

Katoh, Y., and Y. Omura (2004), Acceleration of relativistic electrons due to resonant scattering by whistler mode waves generated by temperature anisotropy in the inner magnetosphere, *J. Geophys. Res.*, *109*, A12214, doi:10.1029/2004JA010654.

Katoh, Y., and Y. Omura (2007), Relativistic particle acceleration in the process of whistler-mode chorus wave generation, *Geophys. Res. Lett.*, *34*, L13102, doi:10.1029/2007GL029758.

Li, W., Y. Y. Shprits, and R. M. Thorne (2007), Dynamic evolution of energetic outer zone electrons due to wave-particle interactions during storms, *J. Geophys. Res.*, *112*, A10220, doi:10.1029/2007JA012368.

Lin, R. P., D. W. Potter, D. A. Gurnett, and F. L. Scarf (1981), Energetic electrons and plasma waves associated with a solar type III radio burst, *Astrophys. J.*, *251*, 364, doi:10.1086/159471.

Lin, R. P., W. K. Levedahl, W. Lotko, D. A. Gurnett, and F. L. Scarf (1986), Evidence for nonlinear wave-wave interactions in solar type III radio bursts, *Astrophys. J.*, *308*, 954, doi:10.1086/164563.

Lu, Q. M., L. Q. Wang, Y. Zhou, and S. Wang (2004), Electromagnetic instabilities excited by electron temperature anisotropy, *Chin. Phys. Lett.*, *21*, 1518, doi:10.1088/0256-307X/21/8/029.

Lu, Q. M., F. Guo, and S. Wang (2006), Magnetic spectral signatures in the terrestrial plasma depletion layer: Hybrid simulations, *J. Geophys. Res.*, *111*, A04207, doi:10.1029/2005JA011405.

Meredith, N. P., R. B. Horne, R. H. A. Iles, R. M. Thorne, D. Heynderickx, and R. R. Anderson (2002), Outer zone relativistic electron acceleration associated with substorm-enhanced whistler mode chorus, *J. Geophys. Res.*, *107*(A7), 1144, doi:10.1029/2001JA900146.

Nishimura, K., S. P. Gary, and H. Li (2002), Whistler anisotropy instability: Wave-particle scattering rate, *J. Geophys. Res.*, *107*(A11), 1375, doi:10.1029/2002JA009250.

O'Brien, T. P., M. D. Looper, and J. B. Blake (2004), Quantification of relativistic electron microburst losses during the GEM storms, *Geophys. Res. Lett.*, *31*, L04802, doi:10.1029/2003GL018621.

Omura, Y., Y. Katoh, and D. Summers (2008), Theory and simulation of the generation of whistler-mode chorus, *J. Geophys. Res.*, *113*, A04223, doi:10.1029/2007JA012622.

Ossakow, S. L., E. Ott, and I. Haber (1972), Nonlinear evolution of whistler instabilities, *Phys. Fluids*, *15*, 2314, doi:10.1063/1.1693875.

Shprits, Y. Y., R. M. Thorne, R. B. Horne, S. A. Glauert, M. Cartwright, C. T. Russell, D. N. Baker, and S. G. Kanekal (2006), Acceleration mechanism responsible for the formation of the new radiation belt during the 2003 Halloween solar storm, *Geophys. Res. Lett.*, *33*, L05104, doi:10.1029/2005GL024256.

Summers, D., and R. M. Thorne (1991), The modified plasma dispersion function, *Phys. Fluids B*, *3*, 1835, doi:10.1063/1.859653.

Summers, D., R. M. Thorne, and F. Xiao (1998), Relativistic theory of wave-particle resonant diffusion with application to electron acceleration in the magnetosphere, *J. Geophys. Res.*, *103*, 20,487, doi:10.1029/98JA01740.

Summers, D., B. Ni, and N. P. Meredith (2007), Timescales for radiation belt electron acceleration and loss due to resonant wave-particle interactions: 1. Theory, *J. Geophys. Res.*, *112*, A04206, doi:10.1029/2006JA011801.

Tao, X., A. A. Chan, J. M. Albert, and J. A. Miller (2008), Stochastic modeling of multidimensional diffusion in the radiation belts, *J. Geophys. Res.*, *113*, A07212, doi:10.1029/2007JA012985.

Thorne, R. M., T. P. O'Brien, Y. Y. Shprits, D. Summers, and R. B. Horne (2005), Timescale for MeV electron microburst loss during geomagnetic storms, *J. Geophys. Res.*, *110*, A09202, doi:10.1029/2004JA010882.

Thorne, R. M., Y. Y. Shprits, N. P. Meredith, R. B. Horne, W. Li, and L. R. Lyons (2007), Refilling of the slot region between the inner and outer electron radiation belts during geomagnetic storms, *J. Geophys. Res.*, *112*, A06203, doi:10.1029/2006JA012176.

Vasyliunas, V. M. (1968), A survey of low-energy electrons in the evening sector of the magnetosphere with OGO 1 and OGO 3, *J. Geophys. Res.*, *73*, 2839, doi:10.1029/JA073i009p02839.

Xiao, F. (2006), Modelling energetic particles by a relativistic kappa loss cone distribution function in plasmas, *Plasma Phys. Controlled Fusion*, *48*, 203, doi:10.1088/0741-3335/48/2/003.

Xiao, F., Q. Zhou, H. Zheng, and S. Wang (2006), Whistler instability threshold condition of energetic electrons by kappa distribution in space plasmas, *J. Geophys. Res.*, *111*, A08208, doi:10.1029/2006JA011612.

Xiao, F., C. Shen, Y. Wang, H. Zheng, and S. Wang (2008), Energetic electron distributions fitted with a relativistic kappa type function at geosynchronous orbit, *J. Geophys. Res.*, *113*, A05203, doi:10.1029/2007JA012903.

Xue, S., R. M. Thorne, and D. Summers (1996), Parametric study of electromagnetic ion cyclotron instability in the Earth's magnetosphere, *J. Geophys. Res.*, *101*, 15,467, doi:10.1029/96JA01087.

Yin, L., M. Ashour-Abdalla, J. M. Bosqued, M. El-Alaoui, and J. L. Bougeret (1998), Plasma waves in the Earth's electron foreshock: 1. Time-of-flight electron distributions in a generalized Lorentzian plasma and dispersion solutions, *J. Geophys. Res.*, *103*, 29,595, doi:10.1029/98JA02294.

Yoon, P. H., C.-M. Ryu, and T. Rhee (2006), Self-consistent formation of electron κ distribution: 1. Theory, *J. Geophys. Res.*, *111*, A09106, doi:10.1029/2006JA011681.

Q. Lu, S. Wang, and L. Zhou, CAS Key Laboratory of Basic Plasma Physics, School of Earth and Space Sciences, University of Science and Technology of China, Hefei, Anhui 230026, China. (qmlu@ustc.edu.cn)